Carbon 123 (2017) 786–793

Contents lists available at ScienceDirect

Carbon

journal homepage: www.elsevier.com/locate/carbon

Graphene welded carbon nanotube crossbars for biaxial strain sensors

Jidong Shi [a, b], Jing Hu [c], Zhaohe Dai [c], Wei Zhao [d], Peng Liu [d], Lingyu Zhao [a, b], Yichuan Guo [a, b], Tingting Yang [e], Liang Zou [a], Kaili Jiang [d], Hongbian Li [a, *], Ying Fang [a, f, **]

[a] CAS Center for Excellence in Nanoscience, National Center for Nanoscience and Technology, Beijing 100190, PR China
[b] University of Chinese Academy of Sciences, Beijing 100049, PR China
[c] Center for Mechanics of Solids, Structures and Materials, Department of Aerospace Engineering and Engineering Mechanics, The University of Texas at Austin, Austin, TX 78712, USA
[d] Department of Physics & Tsinghua-Foxconn Nanotechnology Research Center, Tsinghua University, Beijing 100084, PR China
[e] State Key Laboratory of New Ceramics and Fine Processing, School of Materials Science and Engineering, Tsinghua University, Beijing 100084, PR China
[f] CAS Center for Excellence in Brain Science and Intelligence Technology, 320 Yue Yang Road, Shanghai 200031, PR China

ARTICLE INFO

Article history:
Received 23 May 2017
Received in revised form
20 July 2017
Accepted 3 August 2017
Available online 7 August 2017

ABSTRACT

Aligned carbon nanotube (CNT) arrays are promising candidates for strain sensors owing to their scalable preparation and excellent conductivity and stretchability. However, aligned CNT arrays are limited by low strain sensitivity and buckling deformation. In addition, cross-stacked CNT array films layer-by-layer assembled on soft substrates exhibit anisotropic mechanical behavior due to their asymmetric layered structures. In this work, we introduced a chemically hybridized CNT-graphene (G/CNT) film in which CNT crossbars are effectively welded together by graphene. The hybrid films demonstrate enhanced isotropic mechanical properties and strain sensitivity with a gauge factor of ~3, together with a high stretchability of more than 20%. The enhanced electromechanical properties are attributed to the improved load transfer efficiency among CNTs by graphene hybridization, as confirmed by Finite Element Analysis (FEA). Biaxial strain sensors based on the hybridized G/CNT films have been applied for sensitive detection of both minute vibrations caused by sound waves and large deformations from finger bending. The sensors were further integrated into a tactile sensing array to map the spatial distribution of the surface pressures.

1. Introduction

Flexible and stretchable strain sensors hold significant promise for applications in wearable and implantable electronics [1–10]. Conventional strain sensors based on metal foils or crystalline silicon are limited by low stretchability [11] (maximum strain of 5%). Recently, there have been numerous interests to develop strain sensors by using nanomaterials and their assemblies. In particular, strain sensors based on random CNT networks respond to tensile strains through intertube rotation and sliding [12–15], which leads to large stretchability. Due to their small tube diameter and very low bending stiffness, the CNTs bend and buckle under compressive strains, which results in irreversible deformation and electrical response to cyclic strains [13,16–18]. Reinforcing the strength of the CNT joints can effectively increase their resistance to buckling deformation [18]. However, at the beginning of the tensile deformation, CNTs in a random network tend to rotate and align along the stretching direction [15,19], which results in minimal changes in their conducting pathways and consequently low sensitivity to small strains [20]. As a result, the gauge factors of strain sensors based on both random CNT networks and reinforced random CNT networks are typically below 0.5 [13,15,17,18].

The microstructures of carbon nanotube assemblies play a critical role in defining their collective properties. Compared to random CNT networks, aligned CNT arrays have demonstrated enhanced electrical and thermal conductivity in the parallel direction owing to the alignment effect [20–22]. In addition, continuous, meter-long aligned CNT array films can be readily drawn from as-grown CNT forests [23]. The facile and scalable preparation of aligned CNT array films, combined with their high electrical conductivity [24,25], is essential for their practical applications in strain sensors [26]. In addition, stretchable, cross-stacked CNT films with isotropic

* Corresponding author.
** Corresponding author. National Center for Nanoscience and Technology, Beijing 100190, PR China.
E-mail addresses: lihb@nanoctr.cn (H. Li), fangy@nanoctr.cn (Y. Fang).

http://dx.doi.org/10.1016/j.carbon.2017.08.006
0008-6223/

electrical conductivity have been prepared through the layer-by-layer assembly of aligned CNT arrays in orthogonal orientation [27]. However, these cross-stacked CNT films exhibit anisotropic electromechanical behavior after transferred onto soft substrates, as a result of their asymmetric layered structures and inefficient load transfer in the out-of-plane direction. It is still a challenging task to design CNT-based strain sensors with isotropic sensing properties, as well as high sensitivity and reliability.

In the present study, cross-stacked CNT films have been chemically hybridized with graphene through chemical vapor deposition (CVD), which effectively improves the load transfer efficiency between the two CNT layers. As a result, the hybrid films demonstrate monotonic electromechanical response along both aligned directions, together with a high stretchability of more than 20%. Furthermore, the strain sensitivity of the cross-stacked CNT films has been increased by 5–10 times after graphene hybridization. Multi-functional biaxial strain sensors have been constructed with the G/CNT hybrid films for sensitive detection of both minute vibrations caused by sound waves and also large deformations from finger bending. A sensor array was further integrated for the spatial mapping of the surface pressure.

2. Experimental

2.1. The synthesis of cross-stacked G/CNT films

The film of super-aligned CNT arrays was drawn from vertically aligned CNT forests [23, 28]. The metallic CNTs are multi-walled with diameter of ca. 10 nm. The cross-stacked CNT films were prepared by sequentially stacking two layers of CNT arrays, with the alignment direction perpendicular to each other, which was then scooped up by a Cu foil. The CNT covered Cu foil was loaded into the quartz tube which was then put into in a horizontal Lindberg/Blue furnace (Thermal scientific). The system was then evacuated to $8.0*10^{-2}$ Torr and heated to 1050 °C under a H_2 flow of 8 sccm. After an annealing time of 30 min, a CH_4 flow of 10 sccm was introduced for the growth of graphene. After the graphene growth, the system was cooled down to room temperature with the gases on [29,30].

2.2. The preparation of cross-stacked G/CNT film based strain sensor

The base and curing agent of Polydimethylsiloxane (PDMS, Dow Corning Sylgard 184) were mixed in 10:1 mass ratio. After degassing, the wet PDMS was poured onto a cross-stacked G/CNT film covered Cu and cured at room temperature overnight. The thickness of the PDMS substrate was 2 mm for tensile test and multichannel touch sensing, and was 1 mm for the sound detection test. The Cu foil was then etched with 0.3 mol/L $FeCl_3$ aqueous solution. The membranes were rinsed twice with distilled water to remove $FeCl_3$ residual, and then dried in air. Silver wires were attached to two ends of the cross-stacked G/CNT film for electrical measurements.

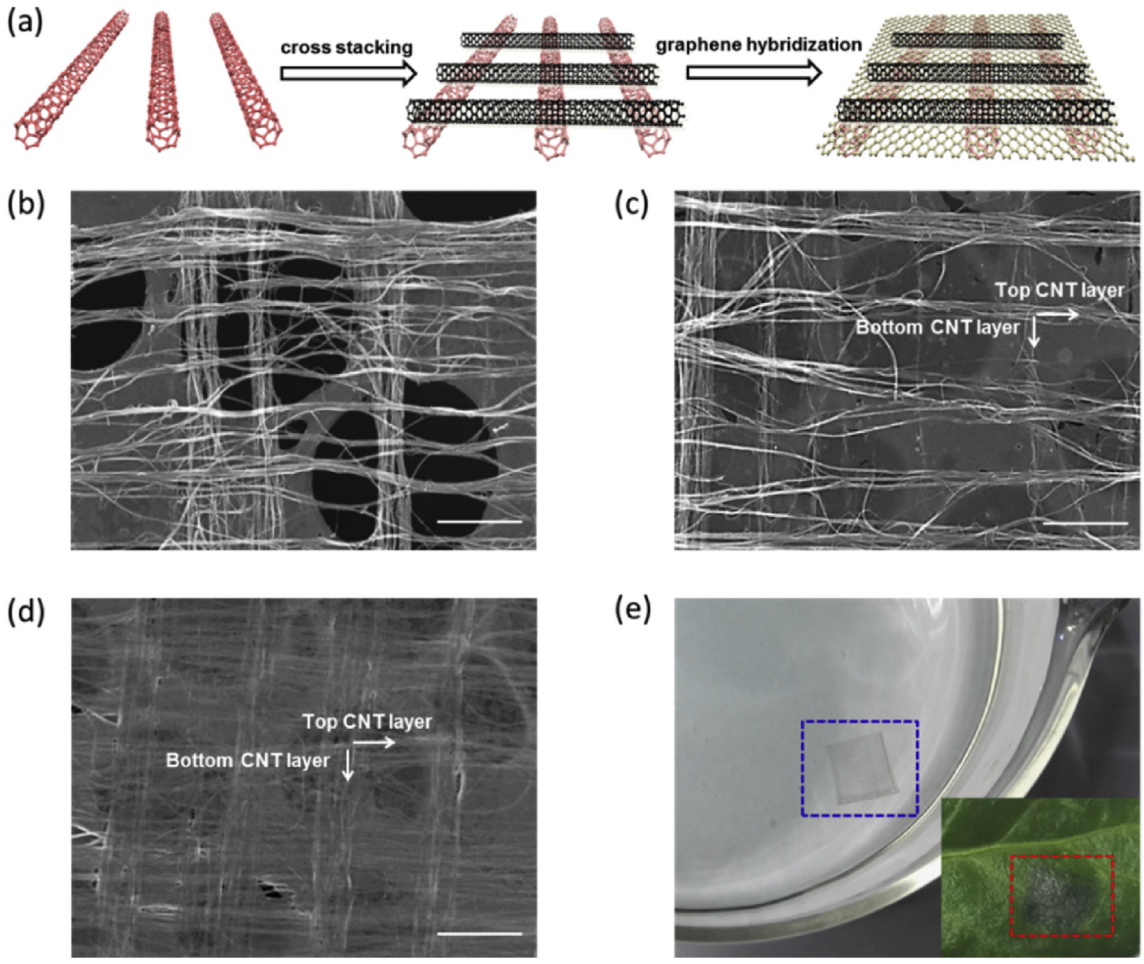

Fig. 1. The preparation of cross-stacked G/CNT hybrids. (a) The schematic of the preparation process. (b) SEM image of a cross-stacked CNT film on Cu grid. (c,d) The SEM images of cross-stacked G/CNT hybrid film on Cu grid from the view of the top and bottom. The alignment direction of different CNT layers is marked by arrows. Scale bar: 2 μm. (e) The optical image showing a freestanding cross-stacked G/CNT film on water. Inset: a cross-stacked G/CNT film conformally contacted onto the rough surface of a leaf. (A colour version of this figure can be viewed online.)

2.3. Mechanical and electrical characterizations

Tensile strains were applied by a dynamic mechanical analyzer manufactured by TA Instruments Company. Resistance recording was conducted in situ by a Keithley 4200-SCS Semiconductor parameter analyzer. The electrical measurements were performed in a two-probe configuration, and DC current was recorded under different strains.

2.4. Morphological analysis

All morphological analysis was conducted by a scanning electron microscopy (SEM, Nova430) manufactured by FEI company.

2.5. The detection of sounds

An ultrathin strain sensor was pasted onto the loudspeaker of a soundbox [31], and the type and sound volume of the music was controlled by a mobilephone through Bluetooth. The control of the sound volume was stepwise, with 13 units including muting (0–12, relatively).

2.6. Finite element analysis simulation

A finite element analysis simulation was conducted in Abaqus. In a representative model, a CNT network consisting of four CNTs in a square pattern is bonded to the PDMS substrate. A quarter of representative model is simulated taking advantage of the plane symmetry of the model. For all of the CNTs, and hybridized graphene, the elastic modulus is 1000 GPa and the Poisson's ratio is 0.16. The CNT is modeled by square cuboid with a cross section of 0.25 m^2. The trapping effect of the bottom layer of cross-stacked CNT film in graphene film is modeled by surface-to-surface contact with infinite elastic slip stiffness. The hybridized graphene is modeled by a block filling in the cross-stacked CNT film and in surface-to-surface contact with two layers and PDMS substrate. The tensile strain is 8% in the horizontal direction. In order to further reveal the deformation of the overall structures as well as the effects of bottom layer on the upper layer in deformation, we also conducted direct loading of the bottom structures. The graphene hybridization with strong molecular-level junction, resulting in the integrated behavior of overall structures, is also modeled by surface-to-surface contact with two CNT layers.

3. Results and discussion

Fig. 1a shows the schematic of the graphene hybridization process of a cross-stacked CNT film. Ultrathin CNT films were firstly drawn from as-grown CNT forests. During the drawing process, CNTs were aligned nearly parallel with the drawing direction. Two layers of aligned CNT films were sequentially stacked on a copper foil in a crossbar structure, which naturally formed a large amount

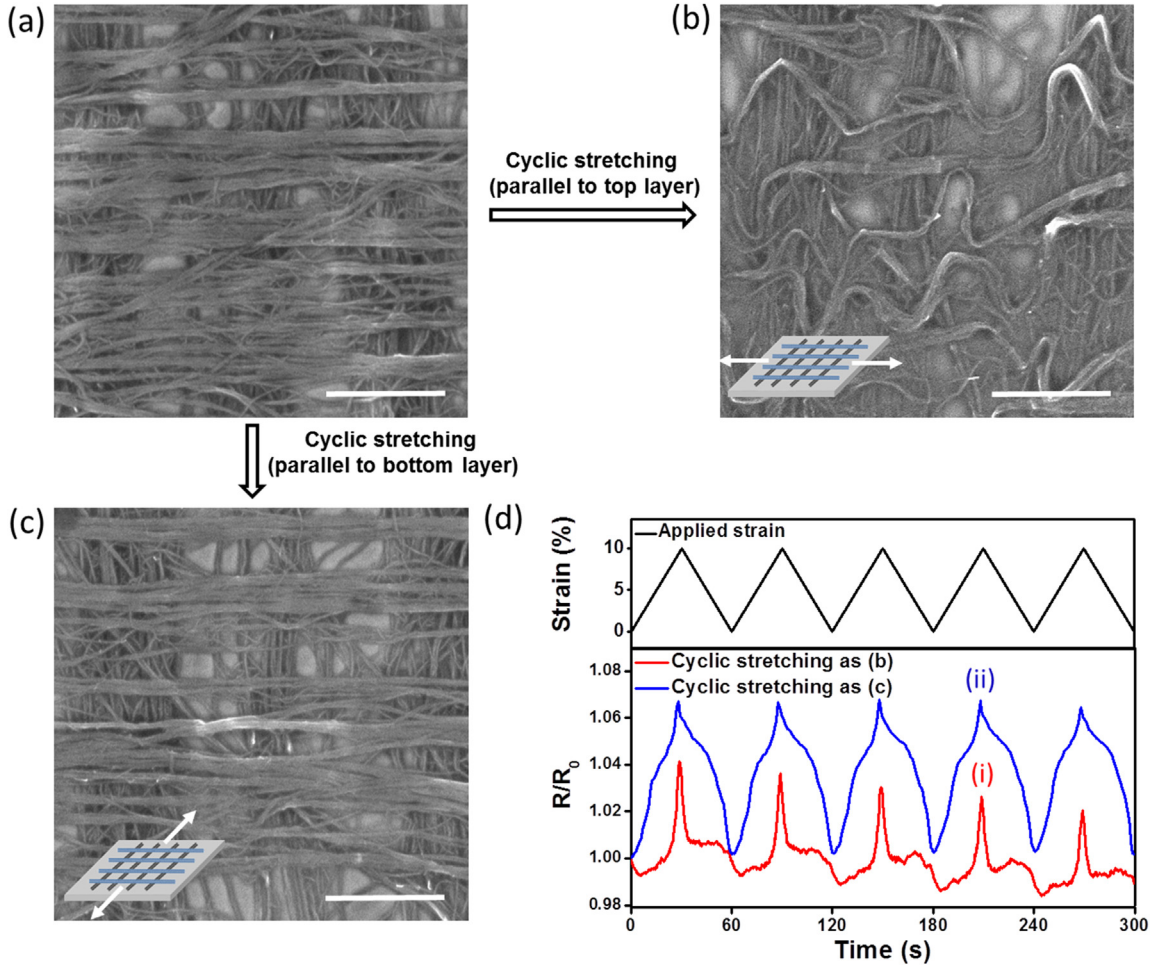

Fig. 2. The morphological evolution and electromechanical response of cross-stacked CNT film upon cyclic stretching with a strain of 10%. (a) The original cross-stacked CNT film on PDMS. (b) Cross-stacked CNT film after cyclic stretching when the stretching direction is parallel to the top and (c) bottom CNT array. Scale bar: 2 μm. (d) The resistance recordings of the cross-stacked CNT film during cyclic stretching with a strain of 10%, with representative 5 consecutive cycles. (A colour version of this figure can be viewed online.)

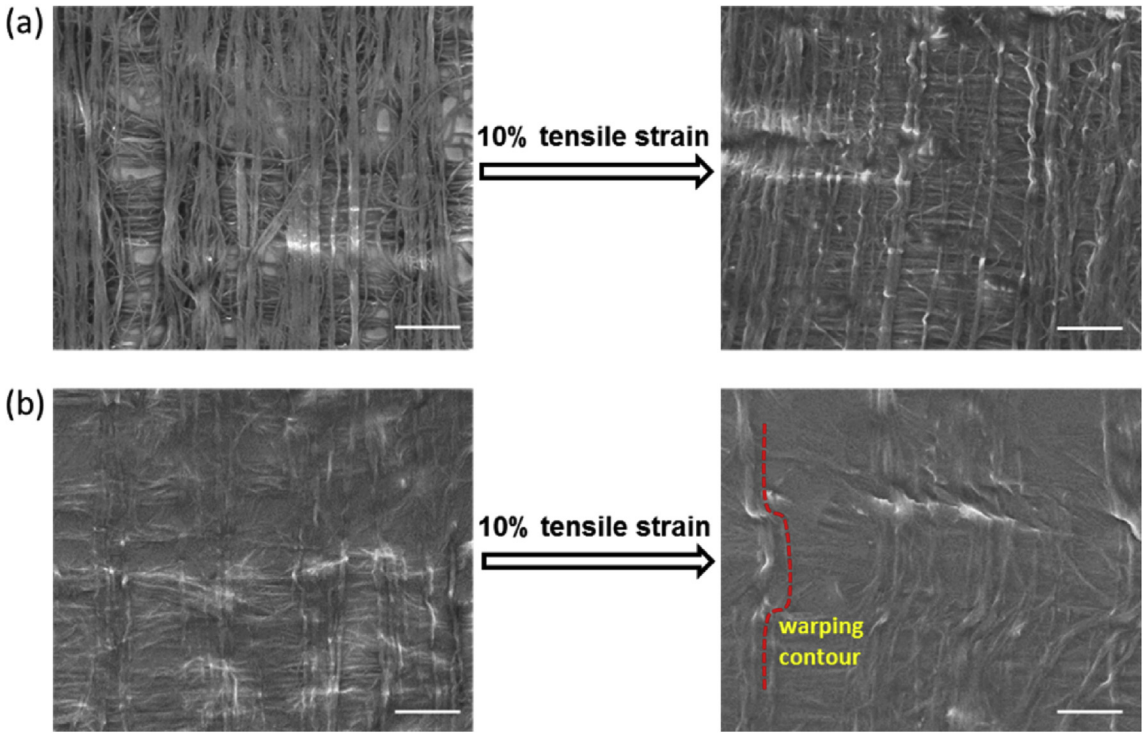

Fig. 3. The morphological evolution of cross-stacked CNT film (a) and cross-stacked G/CNT film (b) upon tensile stretching with a strain of 10%, with stretching direction parallel to the bottom CNT array. Scale bar: 2 μm. (A colour version of this figure can be viewed online.)

of rectangular holes (Fig. 1b). After CVD, graphene filled the nanotube holes, forming a seamless G/CNT hybrid film. Raman characterization shows that the graphene in the hybrid film is mostly monolayer (Fig. S1). As shown in Fig. 1c and d, graphene welded together the bottom and top CNT layers, which greatly enhanced the strength of the cross-stacked CNT film (Fig. S2). Therefore, the freestanding G/CNT hybrid film can be directly transferred onto soft substrates, without the assistance of a polymer stamp. Furthermore, the G/CNT hybrid film is highly flexible and can form conformal contact with a rough surface such as a leaf (Fig. 1e), which is beneficial for their integration into wearable electronics. Moreover, the introduced graphene provides additional conductive pathways, and the sheet resistance of the cross-stacked CNT films decreased from 1335 to 902 Ω/sq after graphene hybridization.

We first investigated the microstructural evolution and the electromechanical response of the cross-stacked CNT films under cyclic stretching. As shown in Fig. 2, a cross-stacked CNT film on soft Polydimethylsiloxane (PDMS) substrate (Fig. 2a) was repeatedly stretched and released with a maximum strain of 10%. When the applied strain was along the orientation of the top CNT layer, extensive buckling occurred in the top CNT layer after cyclic stretching and releasing (Fig. 2b). In contrast, when the applied strain was parallel to the orientation of the bottom CNT layer, no buckling deformation was found (Fig. 2c). The anisotropic microstructural evolution of the cross-stacked CNT film under mechanical strains can be explained by its asymmetrical layered structure and inefficient load transfer between the two CNT layers. When the applied tensile strain was parallel to the orientation of the top CNT layer, the tensile strain caused intertube sliding in the top CNT layer. Upon the release of the tensile strain, CNTs in the top layer bent and buckled under substrate compression due to their high flexibility. On the other hand, the bottom CNT layer was spatially confined between the underlying substrate and the top CNT layer, which greatly suppressed its buckling deformation under cyclic strains.

The aforementioned microstructural evolution of the cross-stacked CNT film led to its anisotropic electrical response to mechanical strains. The resistance of the cross-stacked CNT film was recorded during cyclic stretching and releasing with a maximum strain of 10%. When the applied strain was parallel to the orientation of the top CNT layer, the cross-stacked CNT film showed a weak and non-monotonic resistance response to tensile strains as a result of the irreversible buckling deformation and energy dissipation in the top CNT layer [17,18] (Fig. 2d (i)). On the other hand, when the

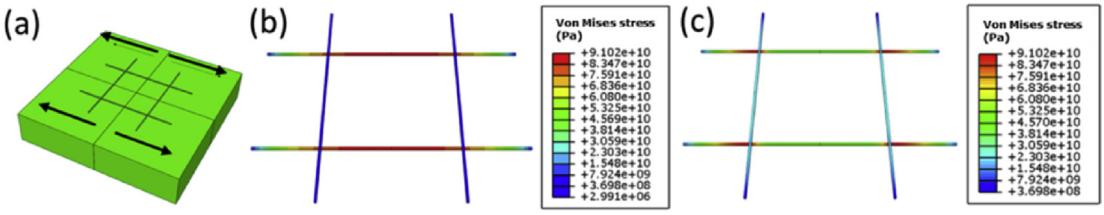

Fig. 4. Finite Element Analysis (FEA) to reveal a better stress transfer after the hybridization of graphene to cross-stacked CNT arrays. (a) Representative model of PDMS supported square CNT networks, with the stretching direction marked by arrows, which is set to be parallel to the bottom layer. (b) The distribution of Mises stress amongst the square CNT network before and (c) after graphene hybridization. (A colour version of this figure can be viewed online.)

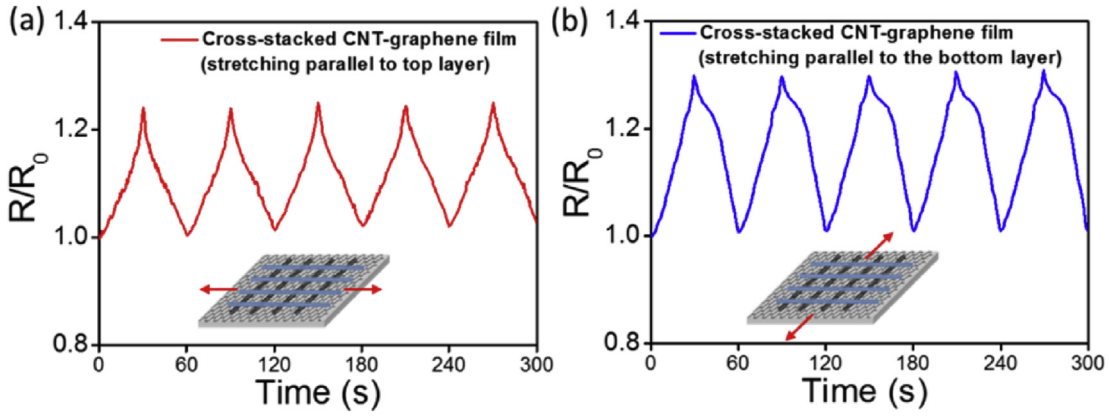

Fig. 5. The electromechanical response of cross-stacked G/CNT film upon cyclic stretching with a strain of 10% when the stretching direction is parallel to the (a) top and (b) bottom CNT array. (A colour version of this figure can be viewed online.)

applied strain was parallel to the orientation of the bottom CNT layer, the cross-stacked CNT film showed a monotonic response to tensile strains because of the suppression of the CNT buckling deformation (Fig. 2d (ii)). We note that similar to random CNT networks, the cross-stacked CNT films are limited by low strain sensitivity. The average gauge factors of the cross-stacked CNT film were measured to be 0.22 and 0.62 along the orientation of the top and bottom CNT layers, respectively. The weak sensitivity and anisotropic electromechanical behavior of the cross-stacked CNT films seriously limit their applications in accurate and reliable strain sensing.

To investigate the role of graphene hybridization, we characterized the microstructures of both the cross-stacked CNT films and G/CNT hybrid films under a tensile strain of 10%. The applied tensile strains were along the orientation of the bottom CNT layers. As shown in Fig. 3a, the 10% tensile strain led to intertube sliding in the bottom CNT layer and lateral separation in the top CNT layer of the cross-stacked CNT film. The CNTs in the top layer of the cross-stacked CNT film were slightly buckled due to the Poisson's effect. On the other hand, the G/CNT hybrid film exhibited a distinctively different microstructure under the same strain value. As shown in Fig. 3b, graphene hybridization effectively welded the top and

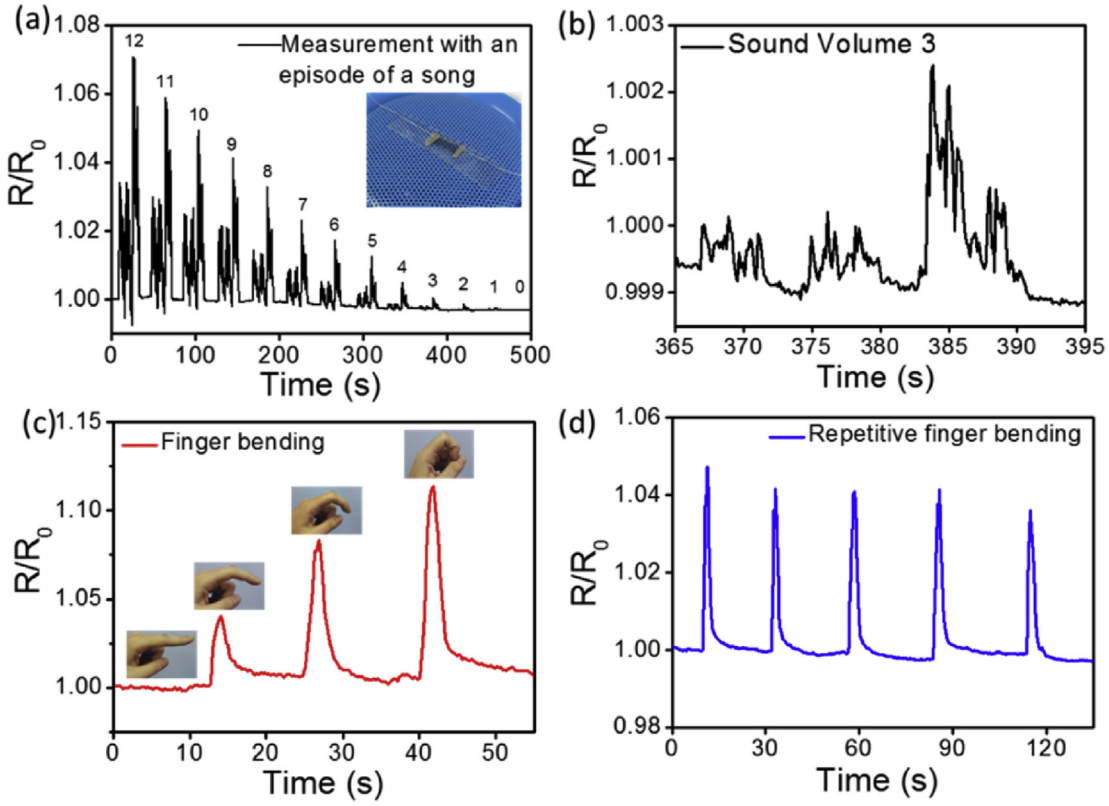

Fig. 6. The application of cross-stacked G/CNT in detecting sounds and joint motions. (a) The resistance recording during the repeated broadcast of a song clip, with the sound volume dropping 1 unit each time. Inset: The photo of a cross-stacked G/CNT based strain sensor adhered on the loudspeaker of a soundbox. (b) The magnified view of the electrical recording of a single song clip, with the sound volume of 3 (unit). (c) The resistance recording of a cross-stacked G/CNT sensor during the bending of a finger with different degrees. (d) The resistance recording during five consecutive bending-unfolding processes of the finger. (A colour version of this figure can be viewed online.)

bottom CNT layers together [32,33], leading to enhanced resistance to shear deformation. As a result, the hybrid film showed extensive warping around the nanotube joints in response to the tensile strain, indicating effective load transfer from the bottom CNT layer to the top CNT layer. In addition, no buckling deformation was observed after cyclic stretching along both alignment directions (Fig. S3).

The effect of graphene hybridization on the enhancement of load transfer within the CNTs was further confirmed by Finite Element Analysis (FEA) (Fig. 4a). In a representative model, a CNT network consisting of four CNTs in a square pattern was bonded onto a PDMS substrate. A model of frictionless layer-to-layer interface with super-lubrication properties was used for the pristine CNT network. While for the graphene welded CNT network, a fixed interface with strong molecular-level junction was employed (See more detail in Methods). The stretching direction was parallel to the orientation of the two CNTs in the bottom layer. As shown in Fig. 4b, the average stress of the CNTs in the top layer of the pristine CNT network was found to be four orders of magnitude lower than that of the bottom CNTs. This poor load transfer between the two CNT layers was due to their nearly frictionless interface [34–36]. Compared to the pristine CNT network, a graphene hybridized CNT network shows dramatically increased average stress in the top CNTs (Fig. 4c). In addition, we further investigated the deformation of the G/CNT hybrid under the twisted stretching of the bottom CNTs using FEA (Fig. S4). The simulated warping structure of the G/CNT hybrid is well consistent with our experimental results in Fig. 3b. These results confirm that graphene hybridization can effectively reinforce the CNT crossbars and enhance the load transfer efficiency between the top and bottom layer CNTs.

As a result of their improved load transfer efficiency, the G/CNT hybrid films exhibit greatly enhanced electromechanical performance. We recorded the resistance of a G/CNT hybrid film during cyclic stretching and releasing with a maximum strain of 10%. As shown in Fig. 5a and b, the G/CNT hybrid film showed relatively isotropic and linear response to mechanical strains along both alignment directions, owing to the efficient load transfer and the prevention of buckling deformation in the hybrid film [17,18]. The effect of graphene in matrix reinforcement and electromechanical linearity is in great correspondence in recent literatures [18,32,37]. More importantly, the hybrid film exhibited greatly enhanced strain sensitivity with gauge factors of 2.38 and 2.98 along the two alignment directions, which is 10 and 5 times higher than those of the original CNT crossbars, respectively. Besides, the G/CNT strain sensors have shown stable performance after 100 cycles of stretching (Fig. S5).

The hybridized G/CNT films combine the merits of enhanced strain sensitivity with high stretchability (more than 20%, Figs. S6 and S7), allowing sensitive detection of both small and large strains. For example, strain sensors based on the hybridized G/CNT films can be used to detect acoustic pressure vibrations of the air [31,38]. Fig. 6a presents the resistance response of a G/CNT strain sensor when a piece of music was played. The acoustic information of the music piece can be accurately and reliably resolved by the G/CNT strain sensor at different volume levels. Fig. 6b shows the detailed resistance changes measured at volume 3. Importantly, the minimum detected strain by the sensor was calculated to be less than 0.01%. In addition, the sound pressure (A1 tone, 55 Hz) was measured to be only 0.15 Pa at volume 3 (Fig. S8). These results highlight the capability of the G/CNT strain sensor for the detection

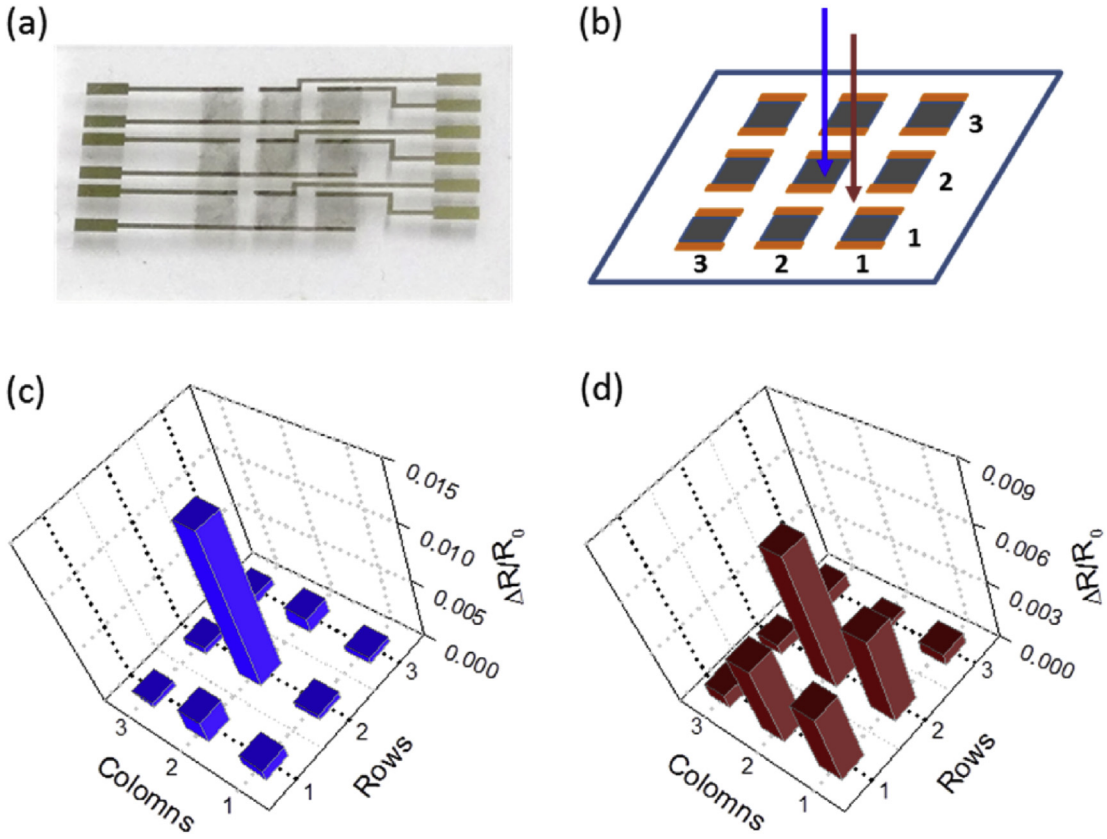

Fig. 7. The application of cross-stacked G/CNT film for multichannel touch sensing. (a) The photo of a 3 × 3 panel of cross-stacked G/CNT film. (b) The schematic of the 3 × 3 touch panel, including the position of electrodes and the representative touch position, indicated by colored arrows. (c) and (d) The electrical response of the touch panel when a point press is applied, with the correspondence of colors in (b). (A colour version of this figure can be viewed online.)

of ultra-small strains. In addition, the G/CNT strain sensors can be also applied to detect large strains induced by human motions [12,39,40]. A G/CNT strain sensor was mounted onto the proximal interphalangeal (PIP) joint of the index finger. The stretching and releasing of the G/CNT strain sensor from the finger bending and straightening motion generated well-defined resistance spikes, and the intensity of the spikes increased with the bending angle of the finger (Fig. 6c). In addition, the strain sensor could work reliably during repeated finger bending process (Fig. 6d).

To detect complex human motions, it is desirable to build strain sensor arrays [41–45]. As a demonstration, we constructed a flexible 3 × 3 tactile sensing array using a hybridized G/CNT film supported on a PDMS substrate (Fig. 7a). The area of each G/CNT sensor was 3 mm × 3 mm, and the center-to-center spacing of adjacent sensors was 4 mm. A point pressure was applied through manual contact on different regions of the sensing array (Fig. 7b). As shown in Fig. 7c and d, the strain outputs of the sensing array corresponded well with the positions of the input pressure. The spatially resolved pressure detection by the G/CNT strain sensor array makes it a promising candidate for the development of integrated e-skins.

4. Conclusion

In summary, cross-stacked CNT films were seamlessly hybridized with graphene through a chemical route. Graphene effectively welded the CNT crossbars together, which greatly enhanced the load transfer efficiency among the CNTs. As a result, the G/CNT hybrid films demonstrated nearly isotropic electromechanical properties. Furthermore, the gauge factor of the G/CNT hybrid films was improved by 5–10 times compared with the cross-stacked CNT films. These characteristics, combined with their good linearity and high stretchability, make the G/CNT hybrid films promising materials for a number of strain sensing applications, including acoustic pressure monitoring and human motion detection.

Conflict of interest

The authors declare no competing financial interest.

Acknowledgements

This work was supported by the National Natural Science Foundation of China (21673057) and the Strategic Priority Research Program of the Chinese Academy of Sciences (XDB02050008). We thank Dr. Yuanchang Li from National Center for Nanoscience and Technology for the discussions, and we thank Ms Suye Lv for her kind help in Raman analysis.

Appendix A. Supplementary data

Supplementary data related to this article can be found at http://dx.doi.org/10.1016/j.carbon.2017.08.006.

References

[1] M.L. Hammock, A. Chortos, B.C.K. Tee, J.B.H. Tok, Z. Bao, 25th anniversary article: the evolution of electronic skin (E-Skin): a brief history, design considerations, and recent progress, Adv. Mater. 25 (42) (2013) 5997–6038.
[2] M. Amjadi, K. Kyung, I. Park, M. Sitti, Stretchable, skin-mountable, and wearable strain sensors and their potential applications: a review, Adv. Funct. Mater. 26 (11) (2016) 1678–1698.
[3] T. Yang, D. Xie, Z. Li, H. Zhu, Recent advances in wearable tactile sensors: materials, sensing mechanisms, and device performance, Mat. Sci. Eng. R 115 (2017) 1–37.
[4] S. Zhao, J. Li, D. Cao, G. Zhang, J. Li, K. Li, et al., Recent advancements in flexible and stretchable electrodes for electromechanical sensors: strategies, materials, and features, ACS Appl. Mater. Inter. 9 (14) (2017) 12147–12164.
[5] S. Yao, Y. Zhu, Nanomaterial-enabled stretchable conductors: strategies, materials and devices, Adv. Mater. 27 (9) (2015) 1480–1511.
[6] W. Chen, X. Gui, B. Liang, R. Yang, Y. Zheng, C. Zhao, et al., Structural engineering for high sensitivity, ultra-thin pressure sensors based on wrinkled graphene and anodic aluminum oxide membrane, ACS Appl. Mater. Inter. 9 (28) (2017) 24111–24117, http://dx.doi.org/10.1021/acsami.7b05515.
[7] C.S. Boland, U. Khan, C. Backes, A. O'Neill, J. Mccauley, S. Duane, et al., Sensitive, high-strain, high-rate bodily motion sensors based on graphene-rubber composites, ACS Nano 8 (9) (2014) 8819–8830.
[8] Z. Chen, Z. Wang, X. Li, Y. Lin, N. Luo, M. Long, et al., Flexible piezoelectric-induced pressure sensors for static measurements based on nanowires/graphene heterostructures, ACS Nano 11 (5) (2017) 4507–4513, http://dx.doi.org/10.1021/acsnano.6b08027.
[9] H. Qi, J. Liu, E. Mäder, Smart cellulose fibers coated with carbon nanotube networks, Fiber 2 (4) (2014) 295–307.
[10] N. Kalashnyk, E. Faulques, J. Schjødt-Thomsen, L.R. Jenson, J.C.M. Rauhe, R. Pyrz, Strain sensing in single carbon fiber epoxy composites by simultaneous in-situ Raman and piezoresistance measurements, Carbon 109 (2016) 124–130.
[11] Y. Kanda, Piezoresistance effect of silicon, Sens. Actuat. A Phys. 28 (2) (1991) 83–91.
[12] T. Yamada, Y. Hayamizu, Y. Yamamoto, Y. Yomogida, A. Izadinajafabadi, D.N. Futaba, et al., Stretchable carbon nanotube strain sensor for human-motion detection, Nat. Nanotechnol. 6 (5) (2011) 296–301.
[13] D.J. Lipomi, M. Vosgueritchian, C.K. Tee, S.L. Hellstrom, J.A. Lee, C.H. Fox, et al., Skin-like pressure and strain sensors based on transparent elastic films of carbon nanotubes, Nat. Nanotechnol. 6 (12) (2011) 788–792.
[14] L. Cai, L. Song, P. Luan, Q. Zhang, N. Zhang, Q. Gao, et al., Super-stretchable, transparent carbon nanotube-based capacitive strain sensors for human motion detection, Sci. Rep. 3 (2013) 3048.
[15] Z. Yu, X. Niu, Z. Liu, Q. Pei, Intrinsically stretchable polymer light-emitting devices using carbon nanotube-polymer composite electrodes, Adv. Mater. 23 (34) (2011) 3989–3994.
[16] Y. Zhu, F. Xu, Buckling of aligned carbon nanotubes as stretchable conductors: a new manufacturing strategy, Adv. Mater. 24 (8) (2012) 1073–1077.
[17] L. Cai, J. Li, P. Luan, H. Dong, D. Zhao, Q. Zhang, et al., Highly transparent and conductive stretchable conductors based on hierarchical reticulate single-walled carbon nanotube architecture, Adv. Funct. Mater. 22 (24) (2012) 5238–5244.
[18] J. Shi, X. Li, H. Cheng, Z. Liu, L. Zhao, T. Yang, et al., Graphene reinforced carbon nanotube networks for wearable strain sensors, Adv. Funct. Mater. 26 (13) (2016) 2078–2084.
[19] M. Park, H. Kim, J.P. Youngblood, Strain-dependent electrical resistance of multi-walled carbon nanotube/polymer composite films, Nanotechnology 19 (5) (2008) 055705.
[20] T.C. Theodosiou, D.A. Saravanos, Numerical investigation of mechanisms affecting the piezoresistive properties of CNT-doped polymers using multi-scale models, Compos. Sci. Technol. 70 (9) (2010) 1312–1320.
[21] M. Zhang, S. Fang, A.A. Zakhidov, S.B. Lee, A.E. Aliev, C.D. Williams, et al., Transparent, multifunctional, carbon nanotube sheets, Science 309 (5738) (2005) 1215–1219.
[22] A. Oliva-Avilés, F. Avilés, V. Sosa, Electrical and piezoresistive properties of multi-walled carbon nanotube/polymer composite films aligned by an electric field, Carbon 49 (9) (2011) 2989–2997.
[23] K. Jiang, Q. Li, S. Fan, Nanotechnology: spinning continuous carbon nanotube yarns, Nature 419 (6909) (2002) 801.
[24] C. Feng, K. Liu, J. Wu, L. Liu, J. Cheng, Y. Zhang, et al., Flexible, stretchable, transparent conducting films made from superaligned carbon nanotubes, Adv. Funct. Mater. 20 (6) (2010) 885–891.
[25] J. Hone, M.C. Llaguno, N.M. Nemes, A.T. Johnson, J.E. Fischer, D.A. Walters, et al., Electrical and thermal transport properties of magnetically aligned single wall carbon nanotube films, Appl. Phys. Lett. 77 (5) (2000) 666–668.
[26] H. Zhu, X. Wang, J. Liang, H. Lv, H. Tong, L. Ma, et al., Versatile electronic skins for motion detection of joints enabled by aligned few-walled carbon nanotubes in flexible polymer composites, Adv. Funct. Mater. 27 (21) (2017) 1606604, http://dx.doi.org/10.1002/adfm.201606604.
[27] K. Liu, Y. Sun, P. Liu, X. Lin, S. Fan, K. Jiang, Cross-stacked superaligned carbon nanotube films for transparent and stretchable conductors, Adv. Funct. Mater. 21 (14) (2011) 2721–2728.
[28] X.B. Zhang, K.L. Jiang, C. Feng, P. Liu, L.N. Zhang, J. Kong, T.H. Zhang, Q.Q. Li, S.S. Fan, Spinning and processing continuous yarns from 4-inch wafer scale super-aligned carbon nanotube arrays, Adv. Mater. 18 (2006) 1505–1510.
[29] X. Li, W. Cai, J. An, S. Kim, J. Nah, D. Yang, et al., Large-area synthesis of high-quality and uniform graphene films on copper foils, Science 324 (5932) (2009) 1312–1314.
[30] E. Shi, H. Li, L. Yang, J. Hou, Y. Li, L. Li, et al., Carbon nanotube network embroidered graphene films for monolithic all-carbon electronics, Adv. Mater. 27 (4) (2015) 682–688.
[31] T. Yang, X. Li, X. Jiang, S. Lin, J. Lao, J. Shi, et al., Structural engineering of gold thin films with channel cracks for ultrasensitive strain sensing, Mater. Horiz. 3 (3) (2016) 248–255.
[32] K.H. Kim, Y. Oh, M.F. Islam, Graphene coating makes carbon nanotube aerogels superelastic and resistant to fatigue, Nat. Nanotechnol. 7 (9) (2012) 562–566. https://www.nature.com/nnano/journal/v7/n9/full/nnano.2012.118.html.

[33] Z. Dai, L. Liu, X. Qi, J. Kuang, Y. Wei, H. Zhu, et al., Three-dimensional sponges with super mechanical stability: harnessing true elasticity of individual carbon nanotubes in macroscopic architectures, Sci. Rep. 6 (2016) 18930.
[34] R. Zhang, Z. Ning, Y. Zhang, Q. Zheng, Q. Chen, H. Xie, et al., Superlubricity in centimetres-long double-walled carbon nanotubes under ambient conditions, Nat. Nanotechnol. 8 (12) (2013) 912–916.
[35] P.L. Dickrell, S.K. Pal, G.R. Bourne, C. Muratore, A.A. Voevodin, P.M. Ajayan, et al., Tunable friction behavior of oriented carbon nanotube films, Tribol. Lett. 24 (1) (2006) 85–90.
[36] A. Kis, K. Jensen, S. Aloni, W. Mickelson, A. Zettl, Interlayer forces and ultralow sliding friction in multiwalled carbon nanotubes, Phys. Rev. Lett. 97 (2) (2006) 025501.
[37] C. Boland, U. Khan, G. Ryan, S. Barwich, R. Charifou, A. Harvey, et al., Sensitive electromechanical sensors using viscoelastic graphene-polymer nanocomposites, Science 354 (6317) (2016) 1257–1260.
[38] S. Gong, W. Schwalb, Y. Wang, Y. Chen, Y. Tang, J. Si, et al., A Wearable and highly sensitive pressure sensor with ultrathin gold nanowires, Nat. Commun. 5 (2014) 3132. https://www.nature.com/articles/ncomms4132.
[39] S.-H. Bae, Y. Lee, B.K. Sharma, H.-J. Lee, J.-H. Kim, J.-H. Ahn, Graphene-based transparent strain sensor, Carbon 51 (2013) 236–242.
[40] C. Yan, J. Wang, W. Kang, M. Cui, X. Wang, C.Y. Foo, et al., Highly stretchable piezoresistive graphene–nanocellulose nanopaper for strain sensors, Adv. Mater. 26 (13) (2014) 2022–2027.
[41] T. Yang, X. Jiang, Y. Zhong, X. Zhao, S. Lin, J. Li, et al., A wearable and highly sensitive graphene strain sensor for precise home-based pulse wave monitoring, ACS Sensor. 2 (7) (2017) 967–974, http://dx.doi.org/10.1021/acssensors.7b00230.
[42] T. Yang, W. Wang, H. Zhang, X. Li, J. Shi, Y. He, et al., Tactile sensing system based on arrays of graphene woven microfabrics: electromechanical behavior and electronic skin application, ACS Nano 9 (11) (2015) 10867–10875.
[43] X. Li, T. Yang, Y. Yang, J. Zhu, L. Li, F.E. Alam, et al., Large-area ultrathin graphene films by single-step Marangoni self-assembly for highly sensitive strain sensing application, Adv. Funct. Mater. 26 (9) (2016) 1322–1329.
[44] S. Liu, X. Wu, D. Zhang, C. Guo, P. Wang, W. Hu, et al., Ultrafast dynamic pressure sensors based on graphene hybrid structure, ACS Appl. Mater. Inter. 9 (28) (2017) 24148–24154, http://dx.doi.org/10.1021/acsami.7b07311.
[45] X. Zhao, Q. Hua, R. Yu, Y. Zhang, C. Pan, Flexible, stretchable and wearable multifunctional sensor array as artificial electronic skin for static and dynamic strain mapping, Adv. Electron. Mater. 1 (7) (2015) 1500142.